Correlation between seismic activity and acoustic emission on the basis of in-situ monitoring

Zhiwen Zhu[1]; Zihan Jiang[1]; Federico Accornero[1]; and Alberto Carpinteri[1]

[1]Department of Civil Engineering and Intelligent Construction, Shantou University, 243 University Road, 515063 Shantou, China

Correspondence: Zhiwen Zhu (zhuzw@stu.edu.cn)

Abstract: Since April 2023 an in-situ experimental campaign has started at a granite underground tunnel, which is a dedicated monitoring platform located in Southeast China. Acoustic Emission (AE) signals and seismic sequences were simultaneously recorded by installing the AE device together with the seismometer, in order to investigate, among other parameters, the b-value and the natural-time variance, κ_1, of AE time series. In addition, AE and related temporal correlation with the incoming seismic events are analyzed using an appropriate multi-modal statistical analysis. The results show that AE has a strong correlation with seismic swarms in surrounding areas. The changing trend of AE temporal distribution occurs before that of the earthquake and regularly anticipates the seismic major event by approximately 17 hours. The AE bursts indicate that an earthquake is approaching. The dense clusters of AE are closely related to two major earthquakes with Richter magnitudes equal to 3.2 and 2.4. Approaching the earthquake occurrence, the b-value shows a downward trend, reaching its minimum value prior to the earthquake, whereas the natural-time variance κ_1 rapidly decreases from 0.07 to a minimum value close to zero. κ_1 occurs earlier than the minimum b-value and the AE bursts. Therefore, trends of the b-value and the natural-time variance derived from the AE time series can be used as effective earthquake precursors. It is also evident that there is widespread micro-seismic activity in the earthquake preparation zone before the earthquake occurrence. The micro-seismic activity represents the origin of microcracks in the nearby ground surface, resulting in the AE bursts. The results of this paper provide new experimental evidence for the application of fracto-emissions as seismic precursors.

1. Introduction

Earthquake precursors are phenomena that take place in advance before the occurrence of an earthquake. These precursors are various, such as ground deformation and stress, changes in Earth tidal strain, geoacoustic and geomagnetic fields, environmental radioactivity, and so on. In the time period before the earthquake occurrence, a very wide area of cracking rocks is active around the epicentre of the upcoming earthquake (Carpinteri et al., 2017). Solids that break in a brittle way are subjected to a rapid emission of mechanical energy, involving the generation of pressure waves that travel at a characteristic speed with the order of magnitude of 10^3 m/s. Assuming a constant pressure wave velocity, the correlation between the wavelength (forming crack) scale and the frequency scale is shown in Fig.1. The frequency range of pressure waves is very wide, from nano-scale defects emitting at the frequency scale of Terahertz (10^{12} Hz), to kilometer-scale fractures emitting at the scale of Hertz (Carpinteri et al., 2017), which is a typical frequency of seismic oscillations and can be detected by sensors arranged on solid bodies. In the framework of Fracture Mechanics, Acoustic Emission (AE) represents a specific part of the strain energy released during the damage process, and it is emitted in the form of transient ultrasonic waves. Prior to an earthquake, AE bursts may result from widespread micro-seismic activity, which propagates through the ground.
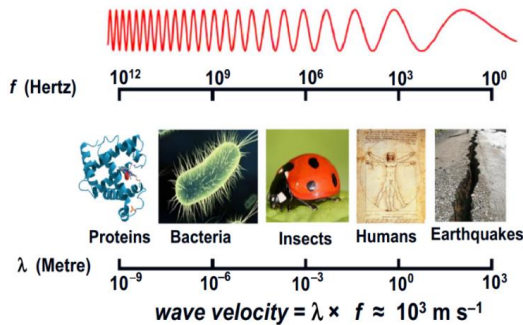
Figure 1. Correlation between wavelength scale and frequency scale (Modified from Carpinteri 2017)

Moreover, according to recent interpretations (Lacidogna et al., 2019), the relationship between crack propagation and
40 emitted energy is represented by the areas subtended by the snap-back instability branches in the load vs displacement diagram
(Fig.2). In Fig.2, the grey areas identify the dissipated energy, D, whereas the pink ones represent the emitted energy, E. The
total energy released during the loading process, R, is equal to the sum of the dissipated energy, D, plus the emitted energy, E.
When an earthquake occurs, AE does not come only from a single macro-crack, but from a wide network of microcracks
generated by micro-seismic activity before the earthquake occurrence. In this way, AE can be effectively used as a seismic
45 precursor.
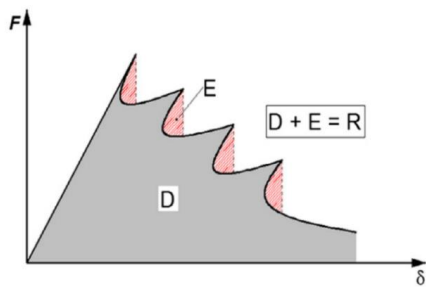
Figure 2. Multiple local instabilities (snap-back) caused by micro-seismic activity

50 An important aspect of earthquake prediction is the dimension and temporal evolution of the "earthquake preparation zone".
Dobrovolsky et al. (1979) assumed that the "strain zone" is a circle with the centre located at the epicentre of the impending
earthquake. The radius R of the circle is called strain radius and is assumed to be a function of the magnitude of the upcoming
earthquake. As an example, for an earthquake with a Richter magnitude M equal to 6, the strain radius is about 1000 kilometers.
Carpinteri et al. (2019) proposed an innovative estimation of the earthquake preparation zone, which is proportional to the
55 magnitude of the upcoming earthquake and depends on the average size of the cracks forming in the Earth's crust before the
seismic event. Approaching the earthquake occurrence, this zone tends to shrink and the pre-existing and external cracks close,
forming a new and smaller preparation zone where the remaining open cracks coalesce to form larger cracks. Therefore, when
the earthquake eventually occurs, the preparation zone will coincide with the earthquake epicentre (Carpinteri et al., 2019).
As shown in Fig.3, in the earlier stages of a seismic event, the preparation zone develops from its maximum size, and, during
60 the first stage, nano- and micro-cracks dominate. In the following stage, as the tectonic stresses tend to get closer to the
earthquake epicentre, the preparation zone will shrink, and the average crack size will increase from the micro-scale to the

millimetre-scale. Approaching the earthquake occurrence, a further size reduction of the preparation zone is expected, characterized by larger cracks, from the millimetre-scale to the metre-scale, which are able to generate ultrasonic acoustic waves up to several hundreds of kHz. At the final stage, the macro-cracks along the seismic fault will coalesce and the earthquake will take place accompanied by audible acoustic emission. Figure 3 shows the evolution of the preparation zone proposed by Carpinteri et al. (2019): each circle represents the evolution of the strain zone. The equivalent crack sizes in the subsequent areas are: 10^{-9}~10^{-6} m (purple), 10^{-6}~10^{-3} m (blue), 10^{-3}~1 m (red), and the black dot is the epicentre of the final earthquake.
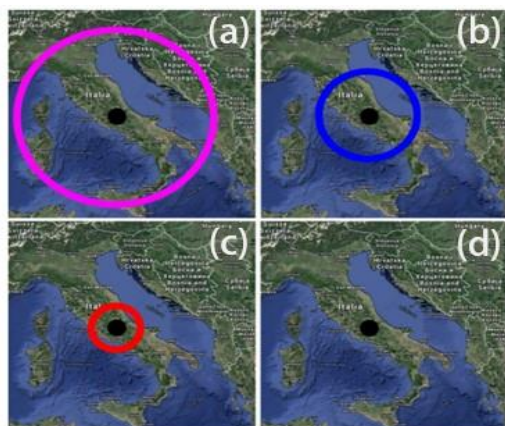
Figure 3. Evolution of earthquake preparation zone (Modified from Carpinteri 2019)

2. AE as seismic precursor

Nowadays, the AE technique is widely used in the field of structural monitoring for civil engineering (Manuello et al., 2019; Han et al., 2019; Dong et al., 2019). In addition, AE can be used as a diagnostic tool in geophysics (Olga et al., 2022; Moriya et al., 2018; Yuri et al., 2023). There are crustal stresses and strains widely distributed within the preparation zone of seismic events (Gregori et al., 2010), and the AE bursts may be interpreted as a characteristic of the crustal stress redistribution (Lacidogna et al., 2011; Carpinteri et al., 2016). AE can be regarded as an earthquake precursor. For example, before the Assisi earthquake, a large and almost sudden burst in AE was observed about 400 kilometers away from the epicentre (Gregori et al., 2005), confirming the fact that AE can be used for earthquake prediction. The correlation between the AE activity in masonry structures and regional earthquakes has been studied by the AE technique (Carpinteri et al., 2013). One of the authors (Lacidogna et al., 2015) proposed a new procedure for earthquake risk assessment based on AE technology, developing statistical methods for space-time correlations between AE and seismic events. In order to evaluate the propagation of in-situ stresses, Zimator et al. (2017) used AE time series obtained from two monitoring stations located about 300 kilometers far apart in Italy. It was found that AE can identify anomalies on crustal stress trend, which may be related to earthquake occurrence. Carpinteri et al. (2017; 2019) installed a monitoring station in a gypsum mine located in northern Italy, where experimental observations show that AE is strongly related to earthquakes occurring in the surrounding area.

In addition, b-value and natural-time variance of AE time series can be used as earthquake precursors. The importance of the b-value for quantifying seismic activity (Allen et al., 1965) or earthquake prediction (Smith et al., 1981) has been widely recognized by seismologists. Sammonds et al. (1992) found that the b-value shows a V-shaped curve with a significant decrement before a major earthquake, whereas most seismic activities occur near the minimum value of the b-value curve.

Han et al. (2015) proposed a robust method for estimating the *b*-value and found that, compared to two traditional methods, this method provides reliable *b*-values and shows good sensitivity to the large-magnitude earthquakes. In addition, the natural-time analysis was proposed only few years ago, and few applications to earthquake prediction are currently presented in the

95   scientific literature. Varotsos et al. (2001) found that, before the occurrence of an earthquake, the seismic activity located in the same tectonic zone would enter a critical stage, whereas the natural-time variance κ_1 fluctuates around the critical value 0.07, decreasing quickly to zero when the earthquake occurs. Sarlis et al. (2013) conducted a study in Japan (25°N~46°N, 125°E~148°E), considering all the earthquakes with magnitude M ≥ 3.5 during the time interval 1984-2011. The results show that for the earthquakes with M ≥ 7.6, κ_1 shows a minimum value before the earthquake occurrence.

100   Since April 2023, an in-situ experimental campaign has started in a granite underground tunnel located in Southeast China. AE signals and seismic sequences were simultaneously recorded, and the AE temporal correlation with the incoming seismic events is analyzed using multi-modal statistical analysis. In addition, the *b*-value and the natural-time variance of AE time series were further investigated. Through the use of the seismometer installed together with the AE device, seismic signals from nearby areas are monitored to record micro-seismic events. Since the monitoring centre is located in a dedicated tunnel,

105   the impact of the environmental ultrasonic noise has been eliminated, such as that coming from traffic, human activities, and wind.

3. In-situ monitoring of AE and earthquakes

An AE and earthquake monitoring system is arranged inside a dedicated tunnel of the seismic monitoring centre of Shantou City. This centre is the backbone station for comprehensive seismic observation in the Eastern region of Guangdong Province,

110   in the Southeast of China. It is located at latitude 23.415°, North, and longitude 116.628°, East (Fig.4). This all-granite tunnel is excavated horizontally into the mountain up to 150 m, and is mainly used to install seismic observation instruments, detecting seismic data such as crustal deformation and underground fluids. All the seismic station equipment are connected to the National Seismic Monitoring Network.

The AE equipment employed is the ÆMISSION system, as shown in Fig.5. The eight-channel system stores signal

115   parameters, including duration, rise time, energy, amplitude, and ringing count, allowing a continuous AE monitoring for the desired time period. This monitoring device uses eight AE sensors (frequency range 10 kHz - 1 MHz) fixed on the ground surface, together with a seismometer to monitor the seismic activity. In the post-processing stage, AE signals with a duration shorter than 3 µs and containing less than three oscillations across the detection threshold were discarded, filtering out electrical noise. The monitoring started at 12:21 on April 24, 2023, and ended at 11:10 on May 29, 2023, resulting in a continuous

120   monitoring for 35 days (839 hours).
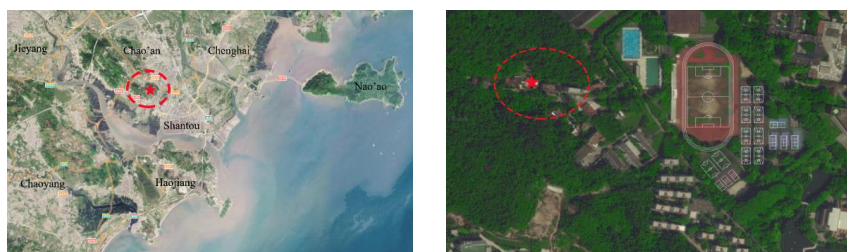
Figure 4. Location of seismic monitoring centre. (a) Shantou seismic station; (b) Detail location of dedicated tunnel

125

Figure 5. Set-up of monitoring system.(a) Interior view of tunnel; (b) AE acquisition device; (c) Seismometer

4. Correlation between seismic and AE activities

4.1 Regional seismic activity

130 Shantou City is a strong earthquake zone in China. The Taiwan Strait, located in the Southeast of Shantou City, is a strong earthquake-prone area with frequently observed moderate to strong earthquakes. The largest reported earthquake in Shantou history occurred in 1918, with a Richter magnitude of 7.9 and epicentre in Nan'ao, an island close to the coast in the South China Sea. The historical seismic activity in the surrounding areas of Shantou is shown in Fig.6. A total of 51 earthquakes with magnitude $M \geq 4.7$ were recorded in the region starting from the year 1067 to 2022, including two earthquakes with

135 magnitudes 7.0-7.9, ten earthquakes with magnitudes 6.0-6.9, 22 earthquakes with magnitudes 5.0-5.9, and 17 earthquakes with magnitudes 4.7-4.9. Since the establishment of the Guangdong Provincial Seismic Network in 1970, only one earthquake of magnitude $M \geq 4.0$ has been recorded in the near-field region, i.e., within 25 kilometers from Shantou, which is the earthquake of magnitude 4.2 in the Chenghai District, occurred on January 16, 2004. Historically, there are three other far-field strong earthquakes near the area: the Quanzhou Earthquake of magnitude 7.1 in 1604, the Haifeng Earthquake of

140 magnitude 6.0 in 1911, and the Taiwan Strait Earthquake of 7.3 magnitude in 1994. In Fig.6, the seismic intensity in this region is generally high. It is worth noting that the vast majority of destructive earthquakes are distributed in the coastal areas of the Eastern continent.
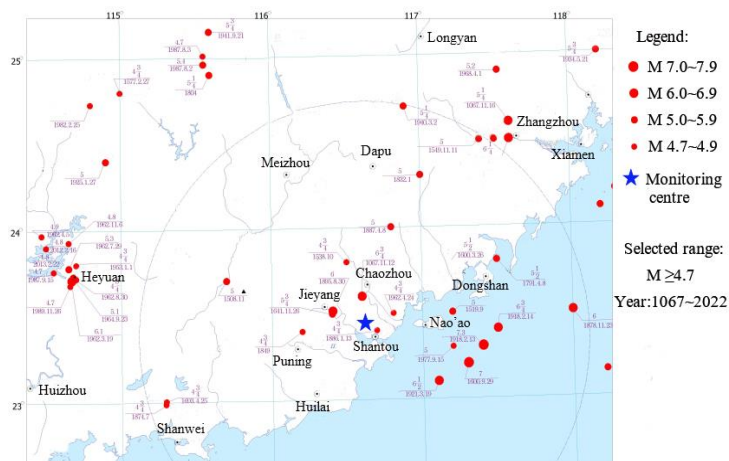
145 Figure 6. Historical seismic activity in area surrounding Shantou City, China

In consideration of the historical seismic activity in the surrounding area, as well as the scale (Dobrovolsky et al., 1979) and time evolution (Carpinteri et al., 2019) of the "earthquake preparation zone" in the pre-earthquake time period, regional earthquakes with epicentre within 200 kilometers from the monitoring centre were selected. During the monitoring time period,

150 small seismic events took place in the area frequently. Based on the magnitude and epicentre distance, two major regional earthquakes are selected: Richter magnitude 3.2 earthquake in Taiwan Strait at 23:50 Beijing Time on April 30, 2023 (EQ.1 for short), and Richter magnitude 2.4 earthquake in Haifeng Sea Area of Guangdong Province at 12:23 Beijing Time on May 17, 2023 (EQ.2 for short). The satellite map showing the location of the two major earthquake is reported in Fig.7. EQ.1 (red dot) has the epicentre 160.1 kilometers far from the monitoring centre (blue dot), whereas EQ.2 (red dot) has the epicentre

155 132.4 kilometers far from the monitoring centre (blue dot). The earthquake information is shown in Table 1.

Table 1. Information about two major earthquakes

Richter Magnitude (M_L)	Date of occurrence	Beijing time	Epicentral distance (km)	Epicentre location	North latitude (°)	East longitude (°)
3.2	April 30, 2023	23:50	160.1	Taiwan Strait	23.37	118.57
2.4	May 17, 2023	12:23	132.4	Haifeng Sea Area	22.83	115.24
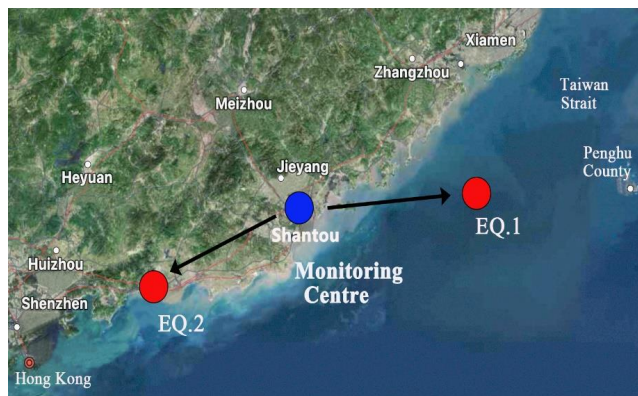
160   Figure 7. Satellite map of epicentres of two major earthquakes

4.2 AE time series and seismic activity

AE rate and seismic sequence during the monitoring time period are shown in Fig.8. AE rate represents the number of AE

events per hour. The blue dots in Fig.8 are the Richter magnitudes (M_L) of the seismic events detected during the monitoring

165   period. The time correlation between AE clusters and seismic events can be observed throughout the monitoring time period.

The dense clusters of AE signals, especially around 142 h and 566 h, show significant peaks in the AE rate, which appear to

anticipate the earthquakes with Richter magnitude equal to 3.2 (EQ.1) and Richter magnitude 2.4 (EQ.2).
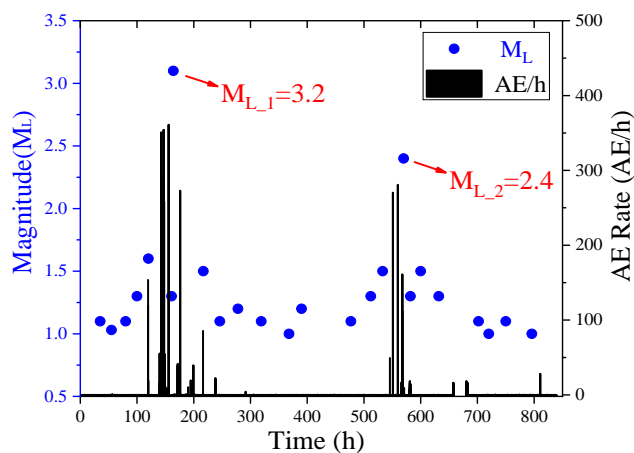
170   Figure 8. AE rate and seismic sequences

The two major earthquakes and the AE time series, including the cumulated AE and the AE rate, are shown in Fig.9. The

cumulated AE represents the total number of AE events occurred during the monitoring period. The times marked by red lines

in Fig.9 are $t_{\_EQ.1}$ (April 30, 2023) and $t_{\_EQ.2}$ (May 17, 2023), which represent the occurrence times of the two major earthquakes.

175   The seismic events are anticipated by large jumps in the cumulated AE and by significant peaks in the AE rate.
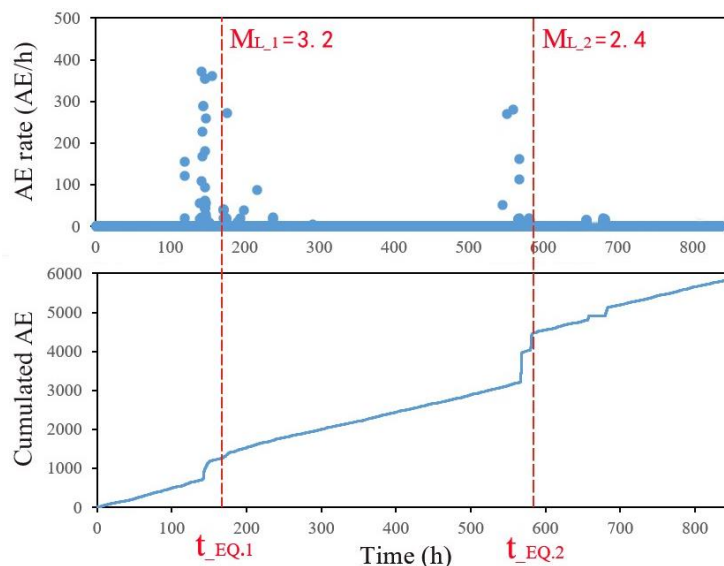
Figure 9. AE rate and cumulated distribution versus seismic events

180   **4.3 Multi-modal statistical analysis**

A multi-modal (Gaussian and multi-peak) statistical analysis is carried out, identifying the relative maxima of AE and seismic

distributions by best Gaussian fitting. In particular, starting from the discrete distribution of data and following an iterative

procedure, in which the curve offset, y_0, centre coordinate, x_c, width, w, and amplitude, A, are considered, the multi-modal

curve that best approximates the discrete distribution of points is identified by the following equations (Fig.10):

185
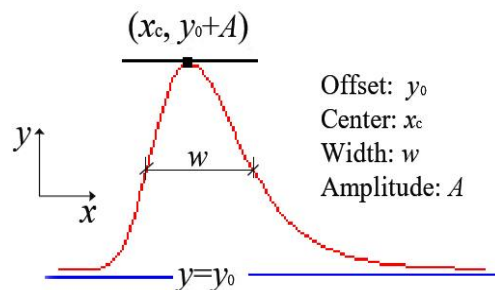
Figure 10. Parameters of the Gaussian curve

$$y = y_0 + Ae^{(-e^{-z}-z+1)}, \tag{1}$$

190 $$z = \frac{x - x_c}{w}. \tag{2}$$

This multi-modal approach is used for the statistical analysis of earthquakes and AE temporal distributions. Regarding the temporal distribution of the 24 earthquakes detected during the 35-day monitoring time period, two major seismic swarms are identified in Fig.11, together with the two AE Gaussian distributions.

The superposition of AE and earthquake distributions is shown in Fig.12, where it is evident the strong correlation between

195 seismic swarms occurring in the monitored area and AE signals, as well as the precursor role played by AE with respect to imminent earthquakes.

Figure 13 clearly shows how AE anticipates each seismic event by approximately 17 hours for both the events.
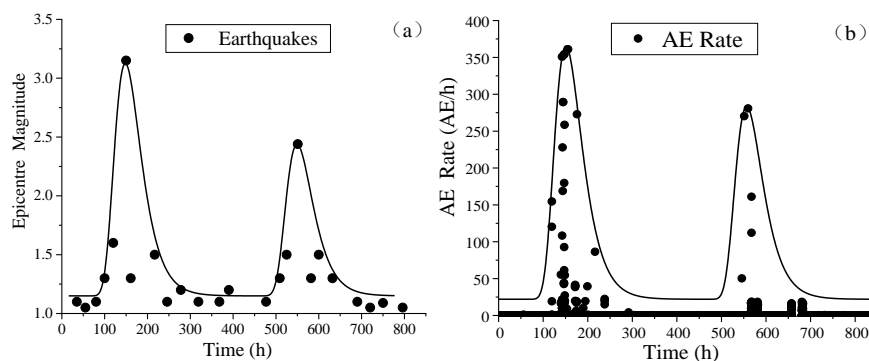
200 Figure 11. Multi-modal Gaussian distribution of earthquakes (a), and AE (b)
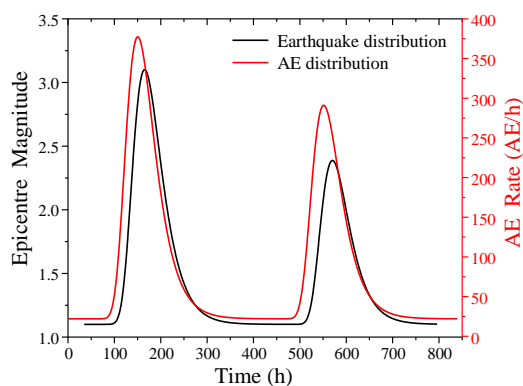
Figure 12. Superposition of Earthquake and AE temporal distributions
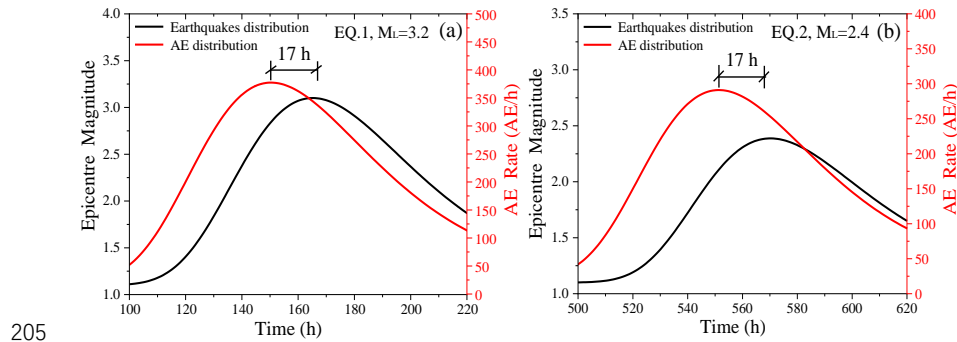
205

Figure 13. Evident role of AE as seismic precursor

4.4 b-value and seismic sequences

Although seismic events exhibit complex space-time behaviour, reflecting the extreme disorder of Earth's crust, universally

210   valid scaling laws emerge. The *b*-value is able to describe the evolution of seismic events by considering the statistical distribution of AE signal magnitude following the Gutenberg–Richter (GR) law (Carpinteri et al., 2011). The GR law was firstly introduced in seismology and then extended to the statistics of AE signals (Colombo et al., 2003):

$$\log_{10}(N_{AE}) = a - bM ,$$
(3)

Where $M = \log_{10}(A_{max})$, A_{max} is the signal peak amplitude, and N_{AE} is the number of AE events with magnitude greater

215   than *M*. The *b*-value is the negative slope of the GR law straight line, which is fitted by the least squares method.

In Fig.14, the AE *b*-values and seismic magnitudes of events EQ.1 and EQ.2 are reported. The occurrence of two major earthquakes resulted in a significant decrement in the *b*-value, reaching a minimum below 1. When approaching the $M_{L\_1}=3.2$ earthquake, the *b*-value drops from 2.3 to 0.9. Then, approaching the $M_{L\_2}=2.4$ earthquake, the *b*-value drops from 2.1 to 0.9. On the other hand, when no major earthquakes occur, the *b*-value tends to increase again. The downward trend of *b*-value can

220   be used as an early warning of earthquakes, the time of minimum *b*-value being just prior to the earthquake occurrence.
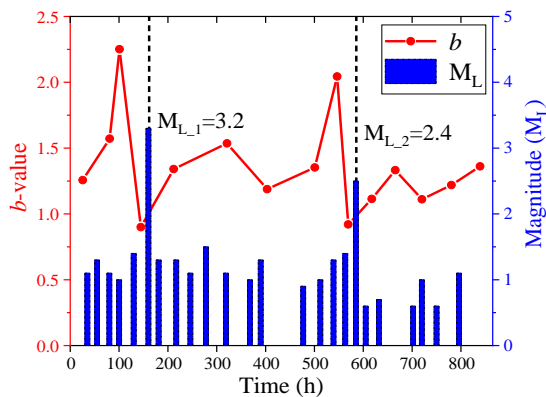
Figure 14. The *b*-value of AE and magnitudes of earthquakes

4.5 Natural-time analysis

Based on the time-series analysis of N events read in a new time domain, namely the natural time, χ , a method to identify critical states was developed (Varotsos et al., 2011 and 2013). The variance κ_1 of the natural time is defined as:

$$\kappa_1 = \sum_{k=1}^{N} p_k \chi_k{}^2 - \left(\sum_{k=1}^{N} p_k \chi_k \right)^2 = \langle \chi^2 \rangle - \langle \chi \rangle^2 , \tag{4}$$

Where $\chi_K = K / N$ is a normalized order of occurrence of the K-th event, and P_K is a probability distribution of the discrete variable χ_K, i.e., a normalized energy. When κ_1 converges to 0.07, the critical state is imminent.

In particular, two conditions have been defined to identify the entrance of the monitored structure to a true critical state (Vallianatos et al., 2013):

(I) The parameter κ_1 approaching the value 0.07 "by descending from above".

(II) The entropies S and S_{rev} lower than the entropy of the uniform noise, which is S_u=0.0966. The entropy s is defined as:

$$S = \langle \chi \ln \chi \rangle - \langle \chi \rangle \ln \langle \chi \rangle, \quad \text{where} \langle \chi \ln \chi \rangle = \sum_{k=1}^{N} \chi_k \ln \chi_k . \tag{5}$$

Similarly, the entropy S_{rev} is obtained by considering the time reversal $T_{PK} = P_{N\_K+1}$.

Therefore, when critical conditions (I) and (II) are satisfied, the moment at which critical state occurs can be justified (Hloupis et al., 2015 and 2016).

Hence, the evolution of variance κ_1, entropy $S,$ and S_{rev} of natural-time series $\{\chi_k\}$ for the seismic event EQ.1 is reported in Fig.15, showing the three variables (κ_1, S, S_{rev}) as functions of time t. The two horizontal dotted lines represent the variance limit κ_1=0.07 and the entropy limit S_u=0.0966, respectively. According to the critical conditions (I) and (II), the value of t_{crit} is shown in Fig.15. In particular, $t_{\_EQ.1}$ represents the occurrence time of the earthquake EQ.1. When approaching the earthquake occurrence, the natural-time variance κ_1 rapidly decreases from 0.07 to a minimum value close to zero.

In addition, a comparison between t_{crit} and $t_{b\text{-}min}$, which is the time characterising the minimum b-value, shows a substantial agreement between the two indicators (see Table 2). The critical time of the variance being earlier than the time of minimum b-value and the time of AE cluster. Thus, the trends of b-value and natural-time variance can be used as seismic precursors.
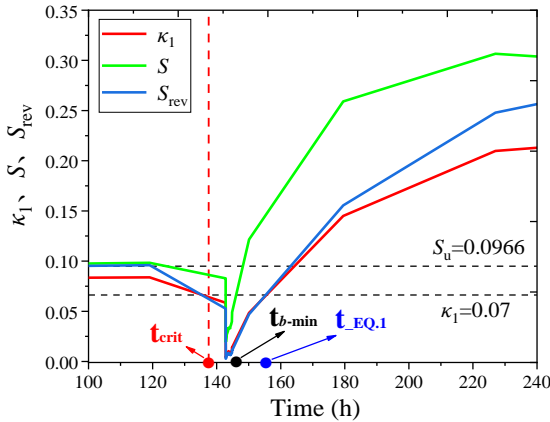
Figure 15. Natural-time series and seismic events

250

Table 2. AE anticipating the seismic event EQ.1

Critical time t_{crit} [h]	Time of AE cluster [h]	Time of minimum b-value, t_{b-min} [h]	Time of the earthquake occurrence $t_{\_EQ.1}$ [h]
139	142	146	155

5.Conclusions and future perspectives

Since April 2023, an in-situ experimental campaign has started at a granite underground tunnel located in Southeast China,
255 revealing the strong seismic forecasting potentialities of the AE peaks by means of a dedicated monitoring platform. The AE and its temporal correlation to the incoming seismic events are analyzed using an appropriate multi-modal statistical analysis. The conclusions are as follows:

(1) The monitoring equipment is arranged in the granite underground tunnel with low noise, and the ideal AE monitoring data and ground motion data are obtained, which indicates the reasonable feasibility of the monitoring system in this paper.

260 (2) The dense clusters of AE, especially around 142 h and 566 h, show large jumps in the cumulated AE and significant peaks in the AE rate, which appear to anticipate the earthquakes with Richter magnitude 3.2 (EQ.1) and the Richter magnitude 2.4 (EQ.2). There was extensive micro-seismic activity before the earthquake occurrence, which may represent the origin of microcracks in the nearby ground surface, resulting in the AE bursts. Thus, AE can be used as seismic precursor.

(3) Multi-modal statistical analysis of earthquake and AE distributions shows that AE has a strong correlation to seismic
265 swarms occurring in surrounding areas. The evaluation trend of AE temporal distribution develops prior to that of the earthquake, and AE tends to anticipate the next seismic peak with an evident and chronologically ordered shifting, which regularly anticipates by approximately 17 hours both the considered seismic events.

(4) b-value analysis shows that, when approaching major seismic events, the b-value decreases significantly and reaches a minimum value below 1, revealing that a larger magnitude event is approaching. The downward trend of b-value can be used
270 as an early warning of earthquakes, the time of minimum b-value being just prior to the earthquake occurrence.

(5) When approaching the earthquake occurrence, the natural-time variance κ_1 rapidly decreases from 0.07 to a minimum value close to zero, the critical time of the variance being earlier than the time of minimum b-value and the time of AE cluster.

Thus, the trends of *b*-value and natural-time variance can be used as seismic precursors.

Current research can only provide time predictions of AE as earthquake precursors, not determining the epicentre and the magnitude of the earthquake. Future studies could identify seismic epicentre and magnitude through the networking of multiple AE devices in different locations. In addition, some other precursory phenomena, such as electromagnetic and neutron emissions, could also be analyzed at the dedicated monitoring platform to provide a more accurate basis for earthquake prediction.

Credit authorship contribution statement

Zhiwen Zhu: Writing – review & editing, Methodology, Investigation, Data curation, Conceptualization. **Zihan Jiang**: Writing – review & editing, Writing – original draft, Methodology, Investigation, Data curation, Conceptualization. **Federico Accornero**: Methodology, Data curation, Conceptualization, Visualization. **Alberto Carpinteri**: Methodology, Supervision, Writing-Review & Editing.

Declaration of competing interest

The authors declare that they have no known competing financial interests or personal relationships that could have appeared to influence the work reported in this paper.

Data availability statement

Data supporting the research obtainable from the corresponding author upon reasonable request.

Acknowledgments

Zhiwen Zhu acknowledges the support from National Natural Science Foundation of China (52278509) and Natural Science Foundation of Guangdong Province (2022A1515 010261). Federico Accornero acknowledges the support from STU Outstanding Talent Grant N. 140-09423016.

References

[1] Carpinteri A, Borla O. Fracto-emissions as seismic precursors. Eng Fract Mech 2017; 177: 239–50. DOI: 10.1016/j.engfracmech.2017.03.007.

[2] Lacidogna G, Accornero F, Carpinteri A. Influence of snap-back instabilities on acoustic emission damage monitoring. Eng Fract Mech 2019; 210: 3–12. DOI: 10.1016/j.engfracmech.2018.06.042.

[3] Dobrovolsky IP, Zubkov SI, Miachkin VI. Estimation of the size of earthquake preparation zones. Pure Appl Geophys 1979; 117(5): 1025–44. DOI: 10.1007/BF00876083.

[4] Carpinteri A, Borla O. Acoustic, electromagnetic, and neutron emissions as seismic precursors: the lunar periodicity of low-magnitude seismic swarms. Eng Fract Mech 2019; 210: 29–41. DOI: 10.1016/j.engfracmech.2018.04.021.

[5] Manuello A, Niccolini G, Carpinteri A. AE monitoring of a concrete arch road tunnel: damage evolution and localization. Eng Fract Mech 2019; 210: 279–87. DOI: 10.1016/j.engfracmech.2018.07.029.

[6] Han QH, Yang G, Xu J, et al. Acoustic emission data analyses based on crumb rubber concrete beam bending tests. Eng

305   Fract Mech 2019; 210: 189–202. DOI: 10.1016/j.engfracmech.2018.05.016.

[7] Dong SF, Zhou DC, Ashour A, et al. Flexural toughness and cal-culation model of super-fine stainless wire reinforced

reaclive pow-der concrele. Cement Concrete Comp 2019, 104: 103367. DOI: 10.1016/j.cemconcomp.2019.103367.

[8] Olga L, Yuri M, Alexandra S. Adaptive approach to time-frequency analysis of AE signals of rocks. Sensors 2022, 22(24):
9798. DOI: 10.3390/s22249798.

310 [9] Moriya H. Acoustic emission/seismicity at depth beneath an artificial lake after the 2011 Tohoku earthquake. Appl Sci
2018, 8(8). DOI: 10.3390/app8081407.

[10] Yuri M, Alexandra S, Olga L, et al. Sound range AE as a tool for diagnostics of large technical and natural objects. Sensors
2023, 23(3): 1269. DOI: 10.3390/s23031269.

[11] Gregori GP Poscolieri M, Paparo G, et al. Storms of crustal stress and AE earthquake precursors. Nat Hazard Earth Syst

315   Sci 2010; 10: 319–37. DOI: 10.5194/nhess-10-319-2010.

[12] Lacidogna G, Carpinteri A, Manuello A, et al. Acoustic and electromagnetic emissions as precursor phenomena in failure

processes. Strain 2011; 47: 144–52. DOI: 10.1111/j.1475-1305.2010.00750.x.

[13] Carpinteri A, Lacidogna G, Manuello A, et al. A study on the structural stability of the Asinelli Tower in Bologna. Struct

Control Health Monit 2016; 23: 659–67. DOI: 10.1002/stc.1804.

320 [14] Gregori GP, Paparo G, Poscolieri M, et al. Acoustic emission and released seismic energy. Nat Hazard Earth Syst Sci

2005; 5: 777–82. DOI: 10.5194/nhess-5-777-2005.

[15] Carpinteri A, Lacidogna G, Invernizzi S, et al. The sacred mountain of Varallo in Italy: Seismic risk assessment by
acoustic emission and structural numerical models. Sci World J 2013; 170291. DOI: 10.1155/2013/170291.

[16] Lacidogna G, Cutugno P, Niccolini G, et al. Correlation between earthquakes and AE monitoring of historical buildings

325   in seismic areas. Appl Sci 2015; 5: 1683–98. DOI: 10.3390/app5041683.

[17] Zimatore G, Garilli G, Poscolieri M, et al. The remarkable coherence between two Italian far away recording stations

points to a role of acoustic emissions from crustal rocks for earthquake analysis. Chaos 2017; 27(4): 043101. DOI:

10.1063/1.4979351.

[18] Allen CR, Amand PS, Richter CF, et al. Relationship between seismicity and geologic structure in the Southern California

330   Region. Bull Seismol Soc Am 1965; 55: 753–97.

[19] Smith WD. The *b*-value as an earthquake precursor. Nature 1981; 289: 136–9.

[20] Sammonds PR, Meredith PG, Main IG. Role of pore fluid in the generation of seismic precursors to shear fracture. Nature
1992; 359: 228–30. DOI: 10.1038/359228a0.

[21] Han QH, Wang LC, Xu J, et al. A robust method to estimate the *b*-value of the magnitude–frequency distribution of

335   earthquakes. Chaos Soliton Fract 2015; 81: 103-10. DOI: 10.1016/j.chaos.2015.09.004.

[22] Varotsos PA, Sarlis NV, Skordas ES. Spatio-temporal complexity aspects on the interrelation between seismic electric

signals and seismicity. Pract Athens Acad Greece 2001; 76: 294–321.

[23] Sarlis NV, Skordas ES, Varotsos PA, et al. Minimum of the order parameter fluctuations of seismicity before major earthquakes in Japan. P Natl Acad Sci USA 2013; 110(34): 13734-8. DOI: 10.1073/pnas.1312740110.

340
[24] Carpinteri A, Lacidogna G, Niccolini G. Damage analysis of reinforced concrete buildings by the acoustic emission technique. Struct Control Health Monit 2011, 18(6):660–73. DOI:10.1002/stc.393.

[25] Colombo IS, Main IG, Forde MC. Assessing damage of reinforced concrete beam using "*b*-value" analysis of acoustic emission signals. J Mater Civ Eng ASCE 2003; 15: 280–6. DOI: 10.1061/(ASCE)0899-1561(2003)15:3(280).

[26] Varotsos PA, Sarlis NV, Skordas ES. Natural time analysis: The new view of time. Springer: Berlin/Heidelberg, Germany,
345
2011. DOI: 10.1007/978-3-642-16449-1.

[27] Varotsos PA, Sarlis NV, Skordas ES, et al. Seismic electric signals: An additional fact showing their physical interconnection with seismicity. Tectonophysics 2013; 589: 116–25. DOI: 10.1016/j.tecto.2012.12.020.

[28] Vallianatos F, Michas G, Benson P, et al. Natural time analysis of critical phenomena: The case of acoustic emissions in triaxially deformed etna basalt. Physica A: Statistical Mechanics and its Applications, 2013, 392(20): 5172-8.
350
DOI:10.1016/j.physa.2013.06.051.

[29] Hloupis G, Stavrakas I, Pasiou ED, et al. Natural time analysis of acoustic emissions in Double Edge Notched Tension (DENT) marble specimens. Procedia Engineering 2015; 109: 248–56. DOI: 10.1016/j.proeng.2015.06.226.

[30] Hloupis G, Stavrakas I, Vallianatos F, et al. A preliminary study for prefailure indicators in acoustic emissions using wavelets and natural time analysis. Proc Inst Mech Eng 2016; 230: 780–8. DOI: 10.1177/1464420715575337.